

# Improving the Electrical Conductivity of Carbon Nanotube Networks: A First-Principles Study

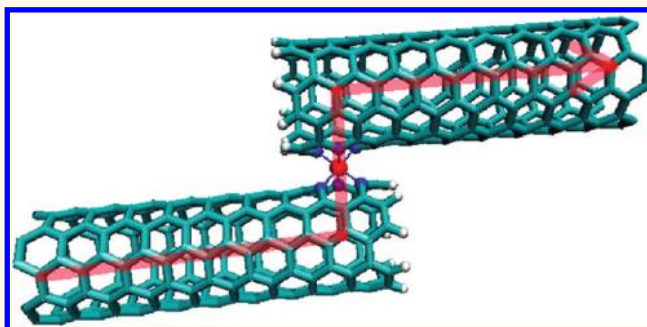
Elise Y. Li<sup>†</sup> and Nicola Marzari<sup>‡,\*</sup>

<sup>†</sup>Department of Materials Science and Engineering, Massachusetts Institute of Technology, Cambridge, Massachusetts 02139, United States and,

<sup>‡</sup>Theory and Simulations of Materials, Ecole Polytechnique Fédérale de Lausanne, CH-1015 Lausanne

While the assembly and connection of individual SWNTs to metal contacts remain challenging for practical applications, carbon nanotube thin films can be readily fabricated and give reproducible characteristics.<sup>1</sup> As a result, there has been increasing enthusiasm to use single-walled carbon nanotube (SWNT) networks as transparent conductive films in various electrochemical applications, ranging from electrodes for solar cells, organic light emitting diodes, and transparent transistors.<sup>2–5</sup> A wide range of conductivities, from 12.5 S/cm<sup>6</sup> to 6600 S/cm<sup>7</sup> have been reported for SWNT films, but regardless of the fabrication methods and SWNT types used, all experimental values are orders of magnitude lower than single SWNT fibers (axial conductivity, ~10000 to 90000 S/cm), owing to poor electronic tunneling at intertube junctions.<sup>7,8</sup> A typical fabrication process for SWNT thin films involves blending the nanotubes into a matrix polymer for good dispersion and suspension, but severely limiting, at the same time, nanotube-to-nanotube carrier hopping. Chemical functionalizations with conductive polymers are commonly employed to improve conductivity, as well as to make mechanically stronger nanocomposites. Nevertheless, most functionalized SWNT networks show further reductions in electrical conductivity by 2 to 3 orders of magnitude due to the interruption of  $\pi$ -conjugation in the tubes, charge trapping, or steric hindrance of bulky functional groups.<sup>7</sup> In the relatively few reported examples where the conductivity of a polymer-nanotube composite does improve, results depend strongly on the morphology and fabrication methods.<sup>9,10</sup> It has also been suggested that conductivity could be dominated by the conductive polymer alone, rather than that of the nanotubes.<sup>10</sup> In any case, neither the nature

## ABSTRACT



We address the issue of the low electrical conductivity observed in carbon nanotube networks using first-principles calculations of the structure, stability, and ballistic transport of different nanotube junctions. We first study covalent linkers, using the nitrene–pyrazine case as a model for conductance-preserving [2 + 1] cycloadditions, and discuss the reasons for their poor performance. We then characterize the role of transition-metal adsorbates in improving mechanical coupling and electrical tunneling between the tubes. We show that the strong hybridization between the transition-metal *d* orbitals with the  $\pi$  orbitals of the nanotube can provide an excellent electrical bridge for nanotube–nanotube junctions. This effect is maximized in the case of nitrogen-doped nanotubes, thanks to the strong mechanical coupling between the tubes mediated by a single transition metal adatom. Our results suggest effective strategies to optimize the performance of carbon nanotube networks.

**KEYWORDS:** first-principles calculations · carbon nanotube networks · quantum conductance · transition metals

of bonding between the CNTs and the polymer linkers nor the mechanism of electron tunneling through a linker at intertube junctions have ever been addressed in detail. Therefore, engineering and optimization of SWNT networks, together with a detailed understanding of their electronic properties, still offer considerable scope for the improvement of SWNT-based electronics.

Many first-principles studies have focused on assembling molecular electronic devices by attaching single molecules between two

\* Address correspondence to nicola.marzari@epfl.ch.

Received for review August 22, 2011 and accepted November 7, 2011.

Published online November 07, 2011  
10.1021/nn2032227

© 2011 American Chemical Society

SWNTs' ends,<sup>11,12</sup> but few have explored the possibility of sidewall functionalizations as an alternative way to cross-link SWNTs. It has been shown that a near-transparent nanotube–molecule–nanotube junction can be obtained through a careful arrangement of the molecular orientation and linkage sites with respect to the tube terminals,<sup>13–16</sup> but the conductivity of such a system would depend strongly on the linker identity, linkage site, molecular conformation, and SWNT chirality. As a result of experimental uncertainties and difficulties in manipulating SWNT–molecule–SWNT junctions at the atomic scale, the observed electric conductance remains poor in most experiments.<sup>11,12,17,18</sup>

As opposed to end functionalizations, sidewall functionalizations have rarely been considered as a possibility to enhance intertube coupling from a theoretical point of view. This can be attributed to the following two reasons: First, most sidewall functionalizations inevitably lead to an unfavorable disruption of the intrinsic nanotube  $sp^2$  conjugation, leading to a strongly decreased electrical performance.<sup>19</sup> Second, the  $\sigma$  bonds of the sidewall functional groups, which are perpendicular to the tube, can hardly be coupled to the  $\pi$  conjugation which runs along the SWNT surface. Nevertheless, for structures like SWNT networks, sidewall functionalizations can offer many more attachment sites and can potentially increase the intertube conductance more effectively than end functionalizations. It would be highly desirable if a sidewall linker could be designed, without the extreme specificity required for end-functionalizations, to serve the same purpose of improving intertube conductivity.

In this study, we use first-principles calculations to address this issue of low electrical conductivity in carbon nanotube networks. We first use polyacene as a prototype model system to study the effect of sidewall linkers on intertube conductivity, and then move on to large scale nanotube calculations. We briefly discuss the nature of intertube tunneling of bare SWNT junctions and the limitation of common covalent linkers. We then explore the effect of transition metal adsorption on CNT surfaces, and find the strong electronic coupling between the transition metals and the sandwiching CNTs, together with strong mechanical coupling, particularly in nitrogen-doped tubes, may lead to novel solutions that have not been considered in this field.

## RESULTS AND DISCUSSION

**Intertube Conductivity of a Polyacene Model.** *Band Structure of a Polyacene Model.* Symmetric (*sym*) polyacene<sup>20</sup> can be seen as the narrowest possible model system which preserves the electronic structure characteristic of a metallic armchair SWNT, marked by the crossing of valence and conduction bands and a quantum conductance of  $2e^2/h$  at the Fermi level. The entire  $p_z$  manifold of *sym*-polyacene is retained in the

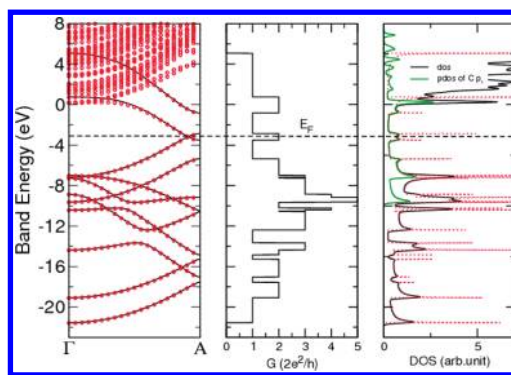


**Figure 1.** Band structure, quantum conductance, and density of states of pristine polyacene. The band structure and density of states calculated from maximally localized Wannier functions are shown in red circles and red dashed lines, respectively. The solid curves represent a fully converged plane-wave basis calculation.

transformation to maximally localized Wannier functions (MLWFs)<sup>21,22</sup> to accurately describe the band dispersion around the Fermi level. Figure 1 shows the Wannier-interpolated band diagram, which matches perfectly the plane wave calculation up to 3 eV above the Fermi energy. The conduction band minimum of polyacene minimum lies 3.14 eV above the Fermi level at the  $\Gamma$  point and exhibits nearly free-electron character, while the  $\pi^*$  bands, strongly hybridized with the  $\sigma^*$  bands, cannot be clearly distinguished, as evidenced by the projected density of states (PDOS) onto all carbon  $p_z$  orbitals (for these reasons the MLWF transformation, containing the full  $p_z$  manifold but not the  $p_x$  or  $p_y$ 's, cannot perfectly trace the physical first unoccupied band close to the  $\Gamma$  point). The Landauer quantum conductance calculated with the MLWFs basis<sup>19</sup> shows the typical step-like behavior with each step corresponding to the sharp Van Hove Singularities of the density of states (DOS).

*Intertube Tunneling without Linkers.* The typical van der Waals mediated distance between two graphene layers in graphite or between CNT tubes in SWNT mats is around 3.5 Å. The intertube transmission, unassisted by cross-linkers, is simulated by laying a short pentacene molecule on top of a broken polyacene junction with both terminals hydrogenated. When the distance between the bridging pentacene is (unphysically) brought to be closer than 2 Å, the substantial hybridization between the  $\pi$  orbitals of the pentacene bridge and the underlying polyacene junction preserves the majority of conductivity around the Fermi level, as shown in Figure 2a. As the distance between the layers is increased, to become larger than 3 Å, the interaction between the  $\pi$  orbitals of the upper and lower layers significantly decreases and the conductance reduces to discrete resonant peaks. The width of the transmission peaks reduces as the interplane distance increases, showing the typical resonant transport characteristics in systems where molecules are only weakly

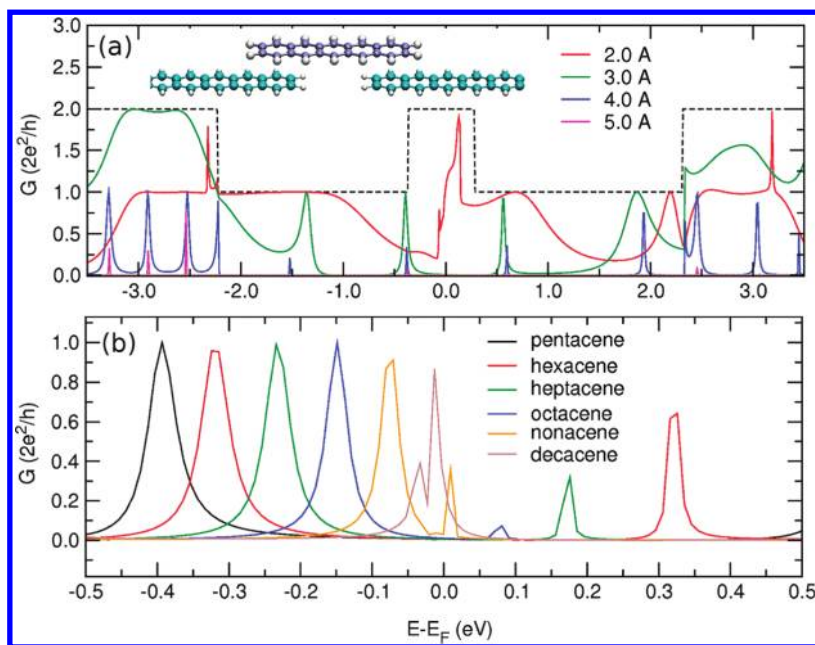


Figure 2. Quantum conductance of a broken polyacene junction bridged by (a) a pentacene molecule with varying adsorption distance (b) different nanoribbon fragments in which the adsorption distance is fixed as 3 Å.

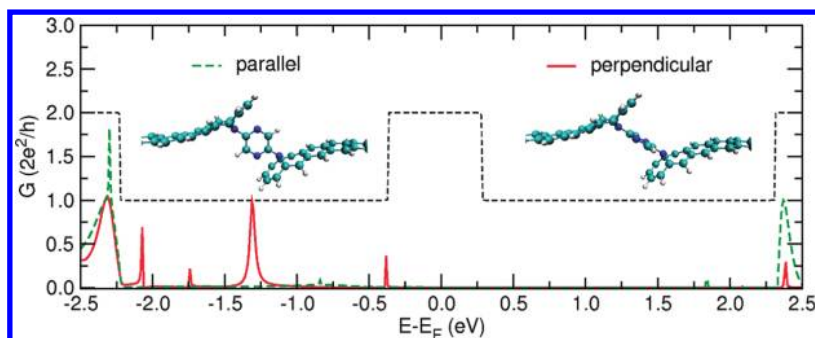
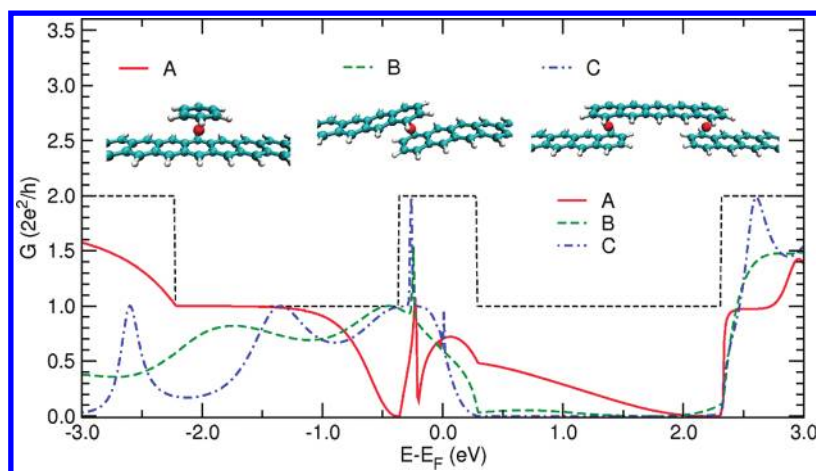


Figure 3. Quantum conductance of a broken polyacene junction bridged by a covalent pyrazine–nitrene linker.

coupled to the leads. The first peak below the Fermi level (0.4 eV) corresponds to the HOMO level (0.37 eV) of isolated pentacene and is right-shifted monotonously toward the Fermi level as the bridging oligoacenes are extended from pentacene to decacene, as can be seen in Figure 2b.

*Intertube Tunneling with Covalent Linkers.* To improve the intertube conductivity by a sidewall organic polymer, an ideal linker must be able to couple the frontier orbitals to those of the nanotubes and must be conductive by itself. It would be best if the linker would preserve the conductivity of pristine CNTs as much as possible, especially for high-degree levels of functionalization. To fulfill all the above criteria, we consider the [1 + 2] cycloadditions of carbenes or nitrenes, which are able to preserve the conductance of the nanotube through sidewall bond cleavage.<sup>23,24</sup> The linker we test on the polyacene model has an aromatic moiety (as in most conductive polymers) substituted with two nitrene groups which connect to the CNT-surface, for example, a nitrene-linked pyrazine. One could hope

that the lone pair  $p_z$  orbital on the nitrene atoms might be able to couple the  $\pi$  orbitals of SWNT to the aromatic  $\pi$  orbitals, and thus increase intertube tunneling. If that were true, then the orientation effect of the pyrazine group would also have a significant effect. We find that the most stable configuration for the pyrazine–nitrene-linked polyacene junction is the one where the pyrazine plane lies perpendicular, rather than parallel, to the polyacene axis, but also that both configurations give essentially zero conductance at the Fermi level (Figure 3). The sparse narrow peaks are characteristic of resonant tunneling and indicate no substantial coupling between two leads. Owing to the relative orientation between the linker and the nanotube, one cannot connect the  $p_z$  orbitals of the two tubes through the  $\pi$  orbitals of the linker, even in the presence of the nitrene lone pair orbital. Furthermore, in this configuration the interpolyacene junction distance is increased from the natural 3.5 to 7 Å, which deteriorates even more the poor tunneling. The scenario corresponds to the experimental situations when



**Figure 4.** Quantum conductance of (A) a pristine polyacene with a bis(benzene)chromium defect, (B) a broken polyacene junction bridged by a chromium atom, and (C) a broken polyacene junction bridged by an adsorbed pentacene and two sandwiched chromium atoms.

the existence of polymer cross-linkers drive CNTs away from each other and undermine electrical conductivity.

#### *Intertube Tunneling with Transition Metal Coupling.*

As an alternative, we shift our focus away from typical organic polymers and turn to coordination chemistry on SWNTs, in particular, sidewall functionalizations *via* coordination with transition metals, inspired by the ferrocene-based molecular wire, are considered here.<sup>25</sup> Transition metals are well-known for their versatile bonding scheme with aromatic systems, including all the sandwich-type metallocenes. It was recently shown experimentally that when two extended polyphenylethynyl fragments are connected by a ferrocene unit in the middle, the conductance at zero source-drain bias is much improved than in the ferrocene-absent analogue, and a broad resonance peak 30 meV above the Fermi level was found in first-principles calculations. This peak arises because the *d* orbitals of the transition metal are close to the Fermi level and interact strongly with the  $\pi$  orbitals of the conjugated backbone. For this reason, we consider first a junction containing a chromium atom since Cr is known to form the stable metallocene bis(benzene)chromium which shares the same hexagonal aromatic moiety as the CNTs.

We examine three structures for polyacene involving Cr coordination and intertube-tunneling, as shown in Figure 4. The relaxed interplane distances are around 3.30 Å for all three systems. The strong hybridization between the Cr *d* orbitals and the polyacene  $\pi$  orbitals acts as a strong scattering center for the perfect polyacene chain (structure A in Figure 4), decreasing the transmission to around 30% of that of the undoped pristine polyacene; for the same reason it also serves as an excellent electrical bridge for broken polyacene segments. All three systems show broad transmission features, with a quantum conductance  $G$  around 0.6 (in units of  $2e^2/h$ ) at the Fermi level and a sharp resonant peak at 0.25 eV below Fermi energy. The eigenchannel

analysis of the transmission spectrum of structure B shown in Figure 5 reveals a conjugated eigenchannel traversing the entire molecule from lead to lead at the Fermi level, giving rise to the observed high transmission. It is evident that the broad band at the Fermi level originates from the HOMO-2 in bis(benzene)chromium, involving a Cr  $d_{xy}$  orbital which strongly couples to the *p* orbitals of both benzene molecules. The resonant peak slightly below the Fermi level corresponds to the HOMO in bis(benzene)chromium with the Cr  $d_{z^2}$  orbital, which only weakly interacts with the benzene  $\pi$  orbitals.

Before we proceed to real carbon nanotube calculations, we would like to discuss the effect that a self-interaction error might exert on our calculations of transport properties,<sup>26</sup> which originates from the incorrect alignment of molecular levels with respect to the Fermi energy of the electrodes, resulting in unphysical peaks on the transmission spectrum. To quantify the eigenvalue energy shifts induced by self-interaction correction, we perform GGA+U calculations on the  $\text{Cr}(\text{C}_6\text{H}_6)_2$  system. The DFT + U method was known to improve the structural and energetic description of some strongly correlated solid-state materials<sup>27,28</sup> as well as isolated transition metal complexes.<sup>29</sup> We find that the eigenvalue of the localized HOMO (mainly Cr  $d_{z^2}$ ) in  $\text{Cr}(\text{C}_6\text{H}_6)_2$ , which is responsible for the sharp resonant peak near the Fermi level in Figure 5, shifts 1.2 eV upward when the *U* is gradually increased from 0 to 5 eV (a typical *U* value for the metallocene systems would be around 2–3 eV). This scenario corresponds to the weak-coupling limit<sup>26</sup> in single molecule transport and will result in a resonant peak energy shift if the self-interaction correction is included. Nevertheless, the molecular orbitals that give rise to the broad feature in the transmission have a very delocalized electron density (*e.g.*, HOMO-1 to HOMO-4) and exhibit a minimal eigenvalue shift (<0.4 eV) even when the *U* value is increased to as large

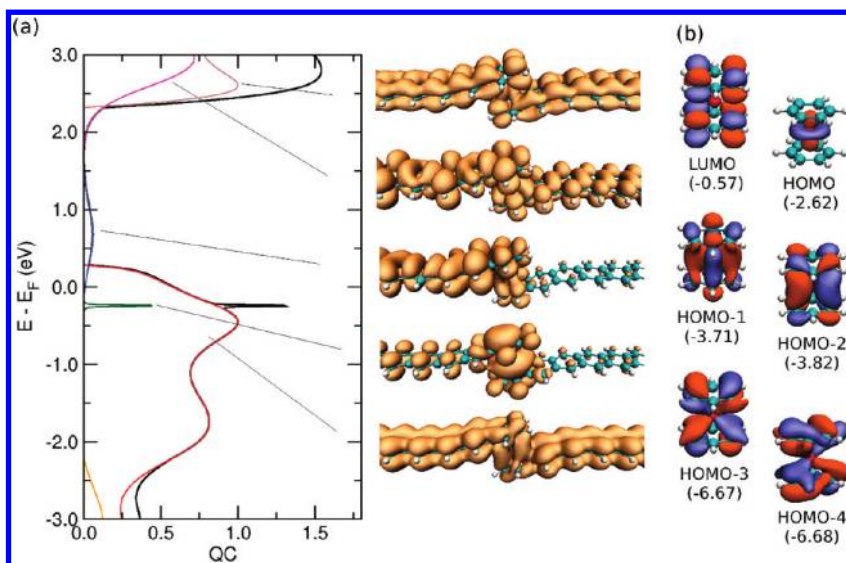


Figure 5. (a) Eigenchannel decomposition and density of the corresponding eigenchannels of quantum conductance for configuration B in Figure 4 near the Fermi level; (b) energy and frontier molecular orbitals of bis(benzene)chromium.

as 5 eV. This corresponds to the strong coupling case<sup>26</sup> where the self-interaction error has a smaller effect. Since the strategy we propose in this study relies on the strongly coupled orbitals between the transition metal and the nanotube  $\pi$  orbitals, we believe that the self-interaction error will have a minimal effect on our systems (*i.e.*, while the sharp resonant peaks might have a non-negligible energy shift, the overall broad feature of the transmission curve will have very small variation). Therefore the following transport calculations done with pure GGA functional should still be valid for subsequent discussions.

**Intertube Conductivity of Carbon Nanotube Junctions.** *Carbon Nanotube Junctions Cross-Linked by Transition Metals.* The bulk conductivity of a macroscopic CNT-network is a complex quantity to predict since it can only be described by percolation models<sup>30</sup> which depend on the length, the morphology, and the atomistic structure at the contacts of the CNTs. The polyacene model discussed up to now shows that the transmission of a broken polyacene junction can be improved dramatically by adding a single transition-metal. Nevertheless, a polyacene chain is only one-benzene wide, so it should not come as a surprise that an  $\eta^6$ -coordinated transition metal atom could connect well the  $\pi$  orbitals between the top and bottom polyacene fragments. CNTs have much larger dimensions and only a small fraction of the  $\pi$  orbitals between two tubes can be directly coupled by a single atom. Thus it becomes fundamental to investigate how much can be achieved by transition-metal coordination in realistic CNT junctions.

Recently, several functionalizations of CNTs have been explored decorating the CNT sidewall with transition metals. In particular, it has been experimentally shown that CNTs nanocomposites doped by transition

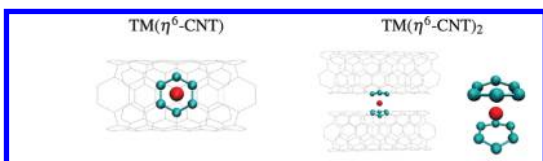
metal (TM) nanoparticles have great potential applications in fuel cells, sensing, catalysis, hydrogen storage, and magnetic nanodevices.<sup>31–35</sup> As for single-atom transition-metal complexes, experimental efforts incorporating iridium, rhodium, and osmium complexes with CNTs have appeared,<sup>36–38</sup> together with theoretical calculations on, for example,  $\text{Cr}(\text{CO})_3$  and  $\text{OsO}_4$  and Vaska's complex.<sup>39–41</sup> Coordination between the transition metals and the CNT  $\pi$  manifold can vary between  $\eta^2$ ,  $\eta^4$ , or  $\eta^6$ , involving two, four, or six  $\pi$  electrons on the CNT surface, respectively, but for most TMs the most stable configuration is the  $\eta^6$ -coordination where the TM atom lies about 1.5 Å above the center of a hexagon, which is the same configuration assumed in the polyacene model. We note in passing that in order for the transition metal to couple the  $\pi$  orbitals between different nanotubes, it must be able to form a local sandwich structure between neighboring CNTs.

We start by calculating the binding energies and stable geometries of a single TM atom adsorbed on a CNT, or sandwiched between two CNTs. The binding geometries are determined by optimizing all atomic positions including the adsorbate atom and 5 carbon rings in a (5,5) CNT (121 or 241 atoms for one or two CNTs, respectively). The first binding energies are obtained when a single TM atom is adsorbed to the surface of a single CNT, from

$$E_b^1 = E_T[\text{CNT}] + E_T[\text{TM}] - E_T[\text{TM} - \text{CNT}] \quad (1)$$

in terms of the total energies of the fully optimized bare nanotube ( $E_T[\text{CNT}]$ ), the free transition metal atom ( $E_T[\text{TM}]$ ), and the TM adsorbed SWNT ( $E_T[\text{TM} + \text{CNT}]$ ), all taken at their lowest magnetic ground states. We define the second binding energy as the energy further released when a second tube is adsorbed to

**TABLE 1.** Calculated Binding Energies ( $E_b^1$  and  $E_b^2$  As Defined in eq 1 and eq 2), Average Carbon–TM Atom Distances ( $d_{TM-C}$ ), and Absolute Magnetization per Unit Cell  $\mu_B$  (the Number of Unpaired Electrons Is Listed Inside the Parentheses) of a Single TM Atom Adsorbed on the Surface of a (5,5) CNT (Left) or between Two (5,5) CNTs (right). A Blow-up of the Local Structure Is Also Shown for the  $TM(\eta^6-CNT)_2$  Sandwich Complex (Right)



Atom	$d_{TM-C}$ (Å)	$E_b^1$ (eV)	$\mu$ ( $\mu_B$ )	$d_{TM-C}$ (Å)	$E_b^2$ (eV)	$\mu$ ( $\mu_B$ )
Sc	2.34	2.04	1.03 (1)	2.42	2.10	1.03 (1)
Ti	2.28	1.97	2.36 (2)	2.34	2.27	2.12 (2)
V	2.31	1.50	4.30 (3)	2.31	2.08	3.46 (3)
Cr	2.47	0.37	6.20 (4)	2.34	1.37	4.85 (2)
Mn	2.54	0.42	6.29 (5)	2.38	1.06	4.99 (3)
Fe	2.25	0.96	4.40 (4)	2.31	1.45	3.09 (2)
Co	2.15	1.26	1.98 (1)	2.29	1.28	3.24 (3)
Ni	2.16	1.56	0	2.39	1.01	0
Cu	2.40	0.38	1.04 (1)	2.42	0.82	1.03 (1)
Zn	4.04	0.05	0	4.11	0.12	0

a TM-decorated CNT, giving rise to the sandwich structure. The second binding energy  $E_b^2$  is

$$E_b^2 = E_T[\text{CNT}] + E_T[\text{TM} - \text{CNT}] - E_T[\text{CNT} - \text{TM} - \text{CNT}] \quad (2)$$

Geometry, binding energies, and magnetic moment of the single TM atom adsorbed to CNTs are presented in Table 1. The calculated values for  $E_b^1$  are comparable to those of a single TM atom adsorbed on a (8,0) or a (6,6) CNT reported in other studies.<sup>42</sup> Owing to the curvature, binding energies are higher for single transition metals adsorbed on SWNT surfaces than on graphene and are in the range of 0 to 2 eV, indicating significant chemisorption. The binding is strongest for early transition metals, such as Sc, Ti, and V, and is weakest for half-filled (Cr, Mn, and Fe) or fully filled TM metals (Cu and Zn). Surprisingly, although Cr is known to form the stable bis(benzene)metallocene, it gives the smallest binding energy (0.37 eV) other than zinc when attached to a single CNT. Further examination reveals that this small binding energy comes from the fact that a free Cr atom has an extremely stable half-filled configuration  $4s^1 3d^5$ , rather than from the formation of a comparatively unstable adsorption structure. The second binding energy  $E_b^2$  is comparable to  $E_b^1$  for most atoms, except in the case of half-filled metals (Cr, Mn, and Fe), where  $E_b^1$  is about 0.5 to 1 eV lower than  $E_b^2$  since the first adsorption event involves a particularly stable free (half-filled) metal atom. The intertube distance in a sandwich structure is around 3.4 Å, also close to the natural  $\pi$ - $\pi$  stacking distance in graphite.

We perform Löwdin population analysis to study the extent of charge transfer from the TM atom to the nanotube. The atomic charges of TM atoms range from

**TABLE 2.** The Calculated Löwdin Atomic Charge of Central Transition Metal Atoms for  $TM(\eta^6-CNT)_x$ ,  $x = 1-2$  (the Structure Shown in Figure 1)<sup>a</sup>

	atomic charge of TM in $TM(\eta^6-CNT)$	atomic charge of TM in $TM(\eta^6-CNT)_2$	oxidation state of TM in $TM(\eta^6-arene)_2$
Sc	0.90	1.04	
Ti	1.10	1.23	Ti(0), <sup>43</sup> Ti(I) <sup>44</sup>
V	0.44	0.30	V(0), <sup>45</sup> V(I) <sup>46,47</sup>
Cr	0.43	0.32	Cr(0), <sup>48-50</sup> Cr(I) <sup>51,50</sup>
Mn	0.33	0.30	Mn(I) <sup>52</sup>
Fe	0.49	0.20	Fe(II) <sup>53</sup>
Co	0.64	0.74	Co(II) <sup>54</sup>
Ni	0.69	0.80	Ni(II) <sup>55</sup>
Cu	0.16	0.33	Cu(I) <sup>56</sup>
Zn	0.01	0.01	

<sup>a</sup> The atomic charge remains unchanged when the length of the CNT is increased from 6 to 12 units in a supercell. The experimental results of the oxidation state of the  $TM(\eta^6-arene)_2$  are also listed.

0 to 1 when a TM atom is adsorbed on the nanotube surface. When the second nanotube is bonded, the atomic charge slightly increases for the early and late transition metals (Sc, Ti, Co, Ni, Cu), and slightly decreases for the half-filled metals (V–Fe). As a comparison, Table 2 also lists the experimental results of the TM oxidation states in  $TM(\eta^6-arene)_2$  complexes. The oxidation states remain relatively low (from 0 to 2+) throughout the first-row TM atoms (note that here the oxidation state  $n$  is also the total charge of the complex,  $TM(\eta^6-arene)_2^{n+}$ ), suggesting that the  $TM(\eta^6-CNT)_2$  structure could possibly exist in the neutral state, or positively charged state when counterions are present. For simplicity, only neutral systems are considered in the following transport calculations.

The interaction strength between a single TM atom and the CNT surface is directly reflected in the quantum conductance calculations, as shown in Figure 6. The conductance of the spin up channel in Figure 6a shows a strong scattering for partially filled 3d transition metals Sc, Ti, V, Cr, Co, and Ni and weak to negligible scattering when the spin up 3d orbitals are completely filled, as is the case in Mn, Fe, and Zn. In the spin down channel, the calculations shows strong scattering for all partially filled 3d metals except for Cu and Zn (6b). The interaction strength can be correlated to the half-width of the transmission "valleys", which represents the extent of scattering when the  $\pi$  channel of a pristine CNT is perturbed by the 3d orbital of the TM. The early transition metals Sc, Ti, V, and Cr show broad features in both the spin up and down channels, compared to other 3d atoms, and are expected to offer a stronger coupling between adjacent nanotubes and a better intertube conductivity in a nanotube junction. Selected atoms are studied in a CNT–TM–CNT sandwich connection configuration, as shown in Figure 7. At first glance it is already remarkable to see that such high intertube quantum

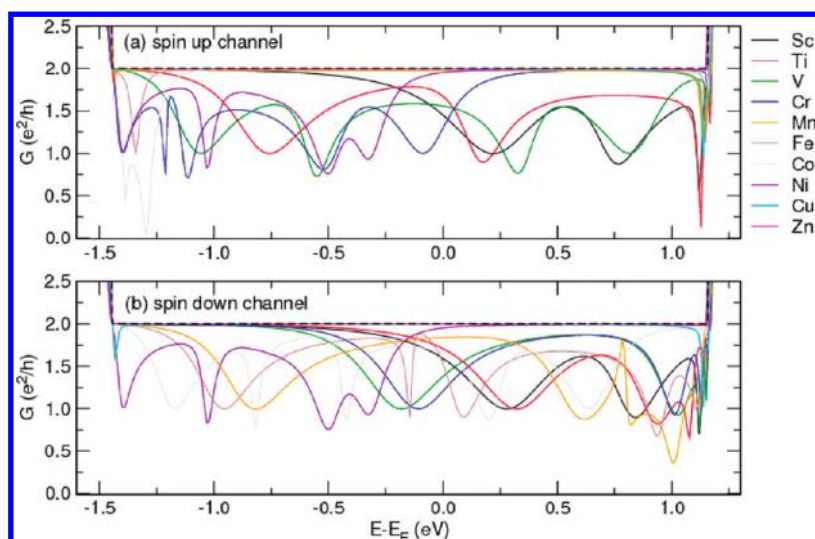


Figure 6. The (a) spin up and (b) spin down quantum conductance near the Fermi level of a (5,5)-CNT scattered by the adsorption of a single first-row transition metal (in the configuration on the left of Table 1). The quantum conductance of a pristine (5,5) CNT is shown by the black dashed curve.

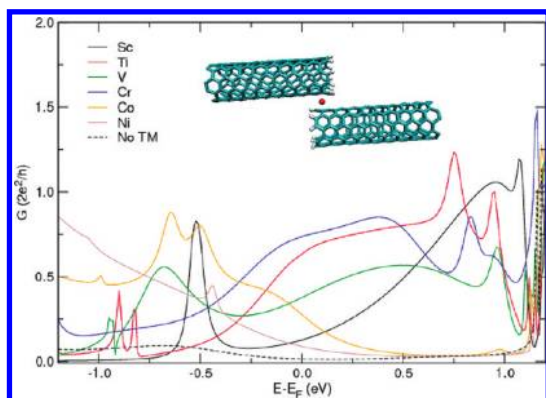


Figure 7. Quantum conductance near the Fermi level of a (5,5)-CNT junction connected by a 3d transition metal. The quantum conductance of the same junction without the transition metal is shown in the "no TM" curve, with the geometry directly taken from the CNT–Cr–CNT structure by removing the central Cr atom, to show the contribution of through space tunneling between the  $\pi$  orbitals unassisted by TM coordination.

conductance can be achieved in a SWNT junction. Of the few metal atoms tested, Ti, V, and Cr show particularly broad transport features around the Fermi level, recovering a quantum conductance up to about  $0.8 G_0$  ( $1G_0 = 2e^2/h$ ) (the quantum conductance of a pristine armchair CNT in this energy window is  $2 G_0$ ). This is a dramatic improvement over unconnected nanotube junctions, which show essentially zero conductance at the Fermi level. Note that in Figure 7 the configuration of the "no TM" junction is taken directly from the CNT–Cr–CNT structure by removing the central Cr atom. In realistic scenarios the intertube conductance of a SWNT junction is likely to be even lower since the tubes would slightly push each other away from the  $3.2 \text{ \AA}$  equilibrium distance between adjacent tubes obtained by the transition-metal bridge in the

CNT–TM–CNT junction. These results also provide one possible explanation for the recent experimental observation that SWNT networks show improved electrical conductivity when doped with Ni, Ir, or Au<sup>57</sup> nanoparticles, even though the size of the nanoparticles (3–5 nm) is considerably larger than the single adatoms we propose in this study.

*Nitrogen-Doped Carbon Nanotube Junctions Cross-Linked by Transition Metals.* Since intertube conductivity of SWNT networks can be greatly improved by transition-metal coordination, the main question left is that if one were able to disperse these adatoms in a network such that neighboring tubes are coupled efficiently through a local sandwich structure. SWNTs have been used as support material for the dispersion and stabilization of metal nanoparticles, and these hybrid materials offer several applications in catalysis, nanoelectronics, and optics.<sup>58,59</sup> Nevertheless, most studies are limited to noble metal nanoparticles, for example, Au, Ag, Pt, Pd, and involve pretreatment on the CNTs, such as acid oxidations, which could impair the electrical and mechanical properties of the CNTs. Alternatively, it has recently been proposed to utilize N-doped CNTs (the CN<sub>x</sub>NTs) as a support material to immobilize various TM nanoparticles. The pyridine-like nitrogen configuration, which has been found to be the favorable structure in CN<sub>x</sub>NTs both from first-principles calculations<sup>60</sup> and XPS measurements,<sup>61,62</sup> could lead to a strong hybridization between single TM atoms and the nitrogen atoms even in the absence of any premodifications.<sup>63</sup>

To quantify the effect of pyridine-like defects to nanotube-TM coupling, we again study the geometry, binding energy, and magnetic moment of a single TM atom adsorbed to CN<sub>x</sub>NTs, as presented in Table 3. The binding energies, geometries and magnetic structure

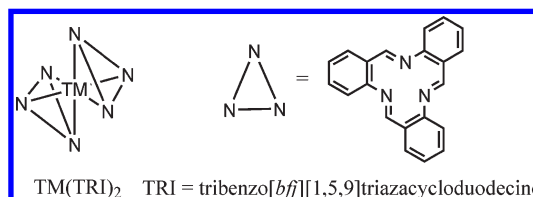
**TABLE 3.** Calculated Binding Energies ( $E_b^1$ ,  $E_b^2$  As Defined in eq 1 and eq 2), Average Nitrogen–TM Atom Distances ( $d_{TM-N}$ ), and the Absolute Magnetization per Unit Cell  $\mu_B$  (the Number of Unpaired Electrons Is Listed Inside the Parentheses) of a Single TM Atom Adsorbed on (Left): the Surface of a (5,5)  $CN_xNT$  or (Right): between Two (5,5)  $CN_xNT$ s. A Blow-up of the Local Structure from a Different Angle Is Also Shown (Right). The Local Structure of the Sandwich Complex Corresponds to a Triaza<sup>12</sup>Annulene Complex

Atom	TM- $CN_xNT$			TM( $CN_xNT$ ) <sub>2</sub>		
	$d_{TM-N}$ (Å)	$E_b^1$ (eV)	$\mu$ ( $\mu_B$ )	$d_{TM-N}$ (Å)	$E_b^2$ (eV)	$\mu$ ( $\mu_B$ )
Sc	2.01	6.83	0	2.19	5.14	1.20 (1)
Ti	1.93	6.69	1.45 (1)	2.12	5.37	0
V	1.91	6.11	3.23 (2)	2.08	4.96	2.71 (3)
Cr	1.88	4.24	4.48 (3)	2.06	4.87	4.06 (4)
Mn	1.94	4.19	5.59 (4)	2.02	3.92	3.19 (3)
Fe	1.87	4.97	4.65 (3)	2.01	3.97	0
Co	1.85	5.20	2.66 (2)	2.02	3.04	1.11 (1)
Ni	1.84	5.04	1.66 (1)	2.11	2.80	2.36 (2)
Cu	1.88	3.81	0	2.17	1.95	1.23 (1)
Zn	2.01	1.73	1.08 (1)	2.18	3.26	0

we find are comparable to those of previous studies of TM metals attached to a pyridine defect on a (10,0) CNT.<sup>64</sup> The first thing to note is that the binding energies of most 3d transition metals to a (5,5)  $CN_xNT$  range from 4 to 6 eV and are on average *three times or higher* compared to the case of attachment to a pristine (5,5) CNT, due to the multiple TM–N bonds formed at the pyridine vacancy sites. Recent first-principles calculations predict a high possibility of forming single TM atom adsorption on these pyridine sites, with an energy barrier for the metal dopant to move to another position on the tube surface estimated to be as high as 7 eV,<sup>64</sup> and is unlikely to happen. The secondary binding energies are also on average *two times higher* than those of CNTs. In addition, the intertube distance of a sandwich structure in the  $CN_xNT$  could be brought to be as close as 3 Å by the transition metal, that is, at least 0.5 Å shorter than the natural  $\pi$ – $\pi$  stacking distance. This indicates that the bonding between the TM atom and the pyridine moiety is strong enough to overcome the natural repulsion between neighboring tubes.

The local structure of the pyridine-like defects in  $CN_xNT$ s resembles well the tridentate Busch macrocycle, the tribenzo[*bff*]<sup>1,5,9</sup>triazacyclododecine (TRI).<sup>65</sup> The TM complexes involving the TRI ligands were studied in the 1960s to the 1980s, and in particular, the  $Co(TRI)_2^{3+}$ ,<sup>66</sup>  $Ni(TRI)_2^{2+}$ ,<sup>67</sup> and  $Cu(MeTRI)_2^{2+}$ <sup>68</sup> have been successfully synthesized. It was found that the bonding between the central metal and the nitrogens is extremely stable and inert to substitution reactions.<sup>68</sup> As shown in the right blow-up in Table 3 and the scheme below, the nitrogen atoms in each TRI ligand

(or the pyridine-like defect in  $CN_xNT$ ) occupy three of the octahedral coordination sites, forming TM–N  $\sigma$  bonds which are intrinsically stronger than the bonding in  $TM(\eta^6\text{-arene})_2$  complexes.



As mentioned earlier, recent studies have shown that the pyridine-type defect is the energetically favored structure among many possible local nitrogen configurations in a nitrogen-doped CNT,<sup>60</sup> and the content of pyridine-like defects can be controlled by the type and ratio of the catalyst used in the synthesis.<sup>69,70</sup> Therefore, contrary to the common expectation that N-doped CNTs shows n-type behavior and greater electron mobility due to the extra electron from the graphitic nitrogen atoms, pyridine-like defects are electron deficient and induce a highly defective trap state near the valence-band edge.<sup>60,71</sup> This causes a large dip near the Fermi level in the transport characteristics of a (5,5)  $CN_xNT$ , as shown in Figure 8. Nevertheless, the quantum conductance of a  $CN_xNT$  is largely recovered by adsorption of a metal atom to the pyridine site, indicating that the damaged  $\pi$  manifold of the tube is restored by TM 3d–nitrogen 2p bonding. Unlike the case of TM-CNTs, where only some species would induce strong scattering in the quantum transport (Figure 6), the transmission of the  $CN_xNT$  is significantly affected by all transition-metal elements, including zinc. Nevertheless, the transmission “dips” of TM-adsorbed  $CN_xNT$ s have narrower half-widths compared to TM-doped CNTs, since the TM metal does not interfere directly with the  $\pi$  orbitals of a CNT atop as in a TM-doped CNTs in the metallocene configuration. The quantum conductance calculation of the  $CN_xNT$  junction connected through the pyridine–TM–pyridine sandwich structure also shows significant improvements, as high as  $1.0 e^2/h$ , as shown in Figure 9. It is found that in this configuration the two tube terminals come extremely close to each other and are only 2.6 Å apart. Therefore it can be expected that the conductance would also include substantial contribution from direct intertube tunneling. Such a short intertube distance is unlikely to exist in real SWNT networks, and a configuration of two pyridine defects on each side unlikely, but an intermediate intertube distance and a TM sandwiching moiety (*i.e.*, a TM coordinated to the  $\eta^6$  ring of one tube and the pyridine site of the other tube) will offer excellent electrical characteristics, intermediate between the two cases discussed.

In summary, we have studied intertube conductivity in a SWNT network with first-principles calculations



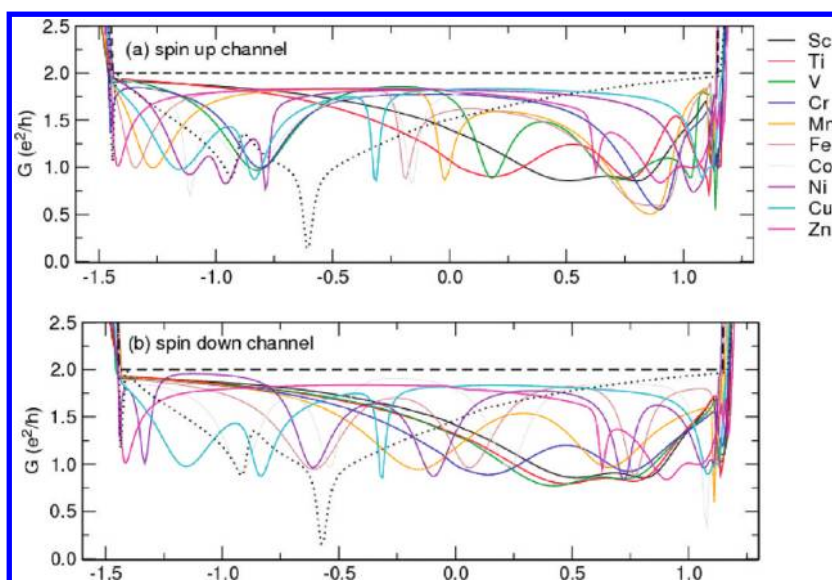


Figure 8. The (a) spin up and (b) spin down quantum conductance near the Fermi level of a (5,5)-CN<sub>x</sub>NT scattered by a single first-row transition metal adsorption (in the configuration of the left insert of Table 3). The quantum conductance of a pristine (5,5) CNT is shown in the black dashed curve; the quantum conductance of a (5,5) CN<sub>x</sub>NT is shown in the black dotted curve.

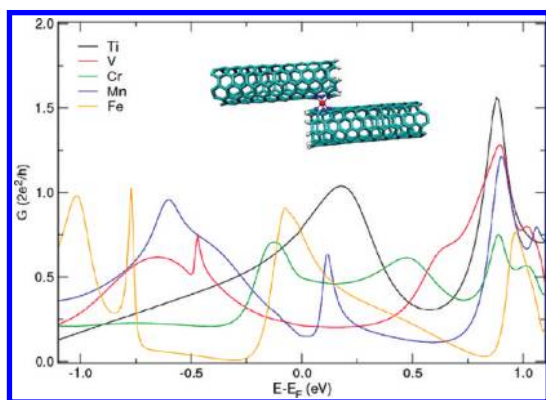


Figure 9. Quantum conductance near the Fermi level of a (5,5)-CN<sub>x</sub>NT junction connected by a 3d transition metal.

on different, paradigmatic model systems. We have discussed the poor characteristics of intertube

tunneling in pristine systems or in the presence of common covalent sidewall functionalizations. We have shown that intertube tunneling can be instead greatly enhanced by transition-metal adsorption on CNT sidewalls, either in pristine or in nitrogen-doped tubes. We studied adsorption geometries and binding energies of first-row transition metals on a (5,5) CNT or sandwiched between two (5,5) CNTs, and also in the presence of nitrogen doping. We find that nitrogen-doped CNTs bind single TM atoms much more strongly, preserving or even improving the excellent transport characteristics of the pristine CNTs. Since such sandwich structures are more likely to be found in TM-doped CN<sub>x</sub>NT networks, these could offer significant enhancements on electrical conductivities of SWNT networks compared with current experimental findings.

## METHODS

**Computational Details.** All calculations are performed using density-functional theory (DFT) in the Perdew-Burke-Ernzerhof generalized-gradient approximation (PBE-GGA)<sup>72</sup> with plane wave basis sets, periodic boundary conditions, and Vanderbilt ultrasoft pseudopotentials<sup>73</sup> as implemented in the Quantum-ESPRESSO package.<sup>74</sup> Ry cutoffs of 30 and 240 or higher are chosen for the wave functions and the charge density, respectively. For isolated molecular systems, a large supercell is constructed so that the distance between periodic images is at least 8 Å to ensure negligible interactions from periodic images. For the carbon nanotube calculations, our supercell includes 5 unit layers of carbon atoms for a given (*n,n*) CNT plus the functional group. A  $1 \times 1 \times 4$  *k*-point sampling is used for structural optimization with a cold smearing of 0.03 Ry.<sup>75</sup> All components of all forces are converged to within  $10^{-3}$  Ry/bohr, corresponding to less than 0.026 eV/Å in a relaxation calculation. Spin-unrestricted DFT formalism is used for open-shell TM-adsorbed nanotube systems and the most stable spin state is identified. The quantum

conductance at zero bias is calculated using the Landauer formalism<sup>76</sup> in a basis of maximally localized Wannier functions (MLWF)<sup>19</sup> as implemented in the Wannier90<sup>77</sup> code. The eigenchannel analysis is obtained with the WanT package.<sup>78,79</sup>

**Acknowledgment.** The authors thank Chesonis Family Foundation and the Department of Energy SciDac program on Quantum Simulations of Materials and Nanostructures (DE-FC02-06ER25794) for funding support.

## REFERENCES AND NOTES

- Wu, Z.; Chen, Z.; Du, X.; Logan, J. M.; Sippel, J.; Nikolou, M.; Kamaras, K.; Reynolds, J. R.; Tanner, D. B.; Hebard, A. F.; Rinzler, A. G. Transparent, Conductive Carbon Nanotube Films. *Science* **2005**, *305*, 1273–1276.
- Artukovic, E.; Kaempgen, M.; Hecht, D. S.; Roth, S.; Grüner, G. Transparent and Flexible Carbon Nanotube Transistors. *Nano Lett.* **2005**, *5*, 757–760.

3. Li, J.; Hu, L.; Wang, L.; Zhou, Y.; Grüner, G.; Marks, T. J. Organic Light-Emitting Diodes Having Carbon Nanotube Anodes. *Nano Lett.* **2006**, *6*, 2472–2477.
4. Grüner, G. Carbon Nanotube Films for Transparent and Plastic Electronics. *J. Mater. Chem.* **2006**, *16*, 3533–3539.
5. Lee, S. W.; Yabuuchi, N.; Gallant, B. M.; Chen, S.; Kim, B.-S.; Hammond, P. T.; Shao-Horn, Y. High-Power Lithium Batteries from Functionalized Carbon-Nanotube Electrodes. *Nat. Nanotechnol.* **2010**, *5*, 531–537.
6. Meitl, M. A.; Zhou, Y.; Gaur, A.; Jeon, S.; Ursey, M. L.; Strano, M. S.; Rogers, J. A. Solution Casting and Transfer Printing Single-Walled Carbon Nanotube Films. *Nano Lett.* **2004**, *4*, 1643–1647.
7. Bekyarova, E.; Itkis, M. E.; Cabrera, N.; Zhao, B.; Yu, A.; Gao, J.; Haddon, R. C. Electronic Properties of Single-Walled Carbon Nanotube Networks. *J. Am. Chem. Soc.* **2005**, *127*, 5990–5995.
8. Cha, S. I.; Kim, K. T.; Lee, K. H.; Mo, C. B.; Jeong, Y. J.; Hong, S. H. Mechanical and Electrical Properties of Cross-Linked Carbon Nanotubes. *Carbon* **2008**, *46*, 482–488.
9. Ma, Y.; Cheung, W.; Wei, D.; Bogozzi, A.; Chiu, P. L.; Wang, L.; Pontoriero, F.; Mendelsohn, R.; He, H. Improved Conductivity of Carbon Nanotube Networks by *in Situ* Polymerization of a Thin Skin of Conducting Polymer. *ACS Nano* **2008**, *2*, 1197–1204.
10. Hermant, M.-C.; van der Schoot, P.; Klumperman, B.; Koning, C. E. Probing the Cooperative Nature of the Conductive Components in Polystyrene/Poly(3,4-Ethylenedioxythiophene): Poly(styrene sulfonate)-Single-Walled Carbon Nanotube Composites. *ACS Nano* **2010**, *4*, 2242–2248.
11. Gue, X.; Small, J. P.; Klare, J. E.; Wang, Y.; Purewal, M. S.; Tam, I. W.; Hong, B. H.; Caldwell, R.; Huang, L.; O'Brien, S.; *et al.* Covalently Bridging Gaps in Single-Walled Carbon Nanotubes with Conducting Molecules. *Science* **2006**, *311*, 356–359.
12. Wei, D.; Liu, Y.; Cao, L.; Wang, Y.; Zhang, H.; Yu, G. Real Time and *in Situ* Control of the Gap Size of Nanoelectrodes for Molecular Devices. *Nano Lett.* **2008**, *8*, 1625–1630.
13. Ke, S.-H.; Baranger, H. U.; Yang, W. Contact Transparency of Nanotube–Molecule–Nanotube Junctions. *Phys. Rev. Lett.* **2007**, *99*, 146802.
14. Qian, Z.; Hou, S.; Ning, J.; Li, R.; Shen, Z.; Zhao, X.; Xue, Z. First-Principles Calculation on the Conductance of a Single 1,4-Diisocyanatobenzene Molecule with Single-Walled Carbon Nanotubes as the Electrodes. *J. Chem. Phys.* **2007**, *126*, 084705.
15. Bruque, N. A.; Ashraf, M. K.; Beran, G. J. O.; Helander, T. R.; Lake, R. K. Conductance of a Conjugated Molecule with Carbon Nanotube Contacts. *Phys. Rev. B* **2009**, *80*, 155455.
16. Martins, T. B.; Fazio, A.; da Silva, A. J. R. Organic Molecule Assembled between Carbon Nanotubes: A Highly Efficient Switch Device. *Phys. Rev. B* **2009**, *79*, 115413.
17. Qi, P.; Javey, A.; Rolandi, M.; Wang, Q.; Yenilmez, E.; Dai, H. Miniature Organic Transistors with Carbon Nanotubes as Quasi-One-Dimensional Electrodes. *J. Am. Chem. Soc.* **2004**, *126*, 11774–11775.
18. Feldman, A. K.; Steigerwald, M. L.; Guo, X.; Nuckolls, C. Molecular Electronic Devices Based on Single-Walled Carbon Nanotube Electrodes. *Acc. Chem. Res.* **2008**, *41*, 1731–1741.
19. Lee, Y.-S.; Marzari, N. Band Structure and Quantum Conductance of Nanostructures from Maximally Localized Wannier Functions: The Case of Functionalized Carbon Nanotubes. *Phys. Rev. Lett.* **2005**, *95*, 076804.
20. Kertesz, M.; Lee, Y. S.; Stewart, J. J. P. Structure and Electronic Structure of Polyacene. *Inter. J. Quan. Chem.* **1989**, *35*, 305–313.
21. Marzari, N.; Vanderbilt, D. Maximally Localized Generalized Wannier Functions for Composite Energy Bands. *Phys. Rev. B* **1997**, *56*, 12847–12865.
22. Shelley, M.; Poilvert, N.; Mostofi, A. A.; Marzari, N. Automated Quantum Conductance Calculations Using Maximally-Localised Wannier Functions. *Comput. Phys. Commun.* **2011**, *182*, year.
23. Lee, Y.-S.; Marzari, N. Cycloaddition Functionalizations to Preserve or Control the Conductance of Carbon Nanotubes. *Phys. Rev. Lett.* **2006**, *97*, 116801.
24. Lopez-Bezanilla, A.; Triozon, F.; Latil, S.; Blase, X.; Roche, S. Effect of the Chemical Functionalization on Charge Transport in Carbon Nanotubes at the Mesoscopic Scale. *Nano Lett.* **2009**, *9*, 940–944.
25. Getty, S. A.; Engtrakul, C.; Wang, L.; Liu, R.; Ke, S.-H.; Baranger, H. U.; Yang, W.; Fuhrer, M. S.; Sita, L. R. Near-Perfect Conduction through a Ferrocene-Based Molecular Wire. *Phys. Rev. B* **2005**, *71*, 241401.
26. Toher, C.; Filippetti, A.; Sanvito, S.; Burke, K. Self-Interaction Errors in Density-Functional Calculations of Electronic Transport. *Phys. Rev. Lett.* **2005**, *95*, 146402.
27. Liechtenstein, A. I.; Anisimov, V. I.; Zaanen, J. Density-Functional Theory and Strong Interactions: Orbital Ordering in Mott–Hubbard Insulators. *Phys. Rev. B* **1995**, *52*, R5467–R5470.
28. Cococcioni, M.; de Gironcoli, S. Linear Response Approach to the Calculation of the Effective Interaction Parameters in the LDA+U Method. *Phys. Rev. B* **2005**, *71*, 035105.
29. Kulik, H. J.; Cococcioni, M.; Scherlis, D. A.; Marzari, N. Density Functional Theory in Transition-Metal Chemistry: A Self-Consistent Hubbard U Approach. *Phys. Rev. Lett.* **2006**, *97*, 103001.
30. Otten, R. H. J.; van der Schoot, P. Connectivity Percolation of Polydisperse Anisotropic Nanofillers. *J. Chem. Phys.* **2011**, *134*, 094902.
31. Liu, H.; Song, C.; Zhang, L.; Zhang, J.; Wang, H.; Wilkinson, D. P. A Review of Anode Catalysis in the Direct Methanol Fuel Cell. *J. Power Sources* **2006**, *155*, 95–110.
32. Star, A.; Joshi, V.; Skarupo, S.; Thomas, D.; Gabriel, J. P. Gas Sensor Array Based on Metal-Decorated Carbon Nanotubes. *J. Phys. Chem. B* **2006**, *110*, 21014–21020.
33. Wu, G.; Chen, Y. S.; Xu, B. Q. Remarkable Support Effect of SWNTs in Pt Catalyst for Methanol Electro Oxidation. *Electrochem. Commun.* **2005**, *7*, 1237–1243.
34. Dag, S.; Ozturk, Y.; Ciraci, S.; Yildirim, T. Adsorption and Dissociation of Hydrogen Molecules on Bare and Functionalized Carbon Nanotubes. *Phys. Rev. B* **2005**, *72*, 155404.
35. Samouhos, S.; McKinley, G. Carbon Nanotube–Magnetite Composites, with Applications to Developing Unique Magnetorheological Fluids. *J. Fluids Eng.* **2007**, *129*, 429–437.
36. Banerjee, S.; Wong, S. S. Functionalization of Carbon Nanotubes with a Metal-Containing Molecular Complex. *Nano Lett.* **2002**, *2*, 49–53.
37. Banerjee, S.; Wong, S. S. Structural Characterization, Optical Properties, and Improved Solubility of Carbon Nanotubes Functionalized with Wilkinson's Catalyst. *J. Am. Chem. Soc.* **2004**, *124*, 8940–8948.
38. Banerjee, S.; Wong, S. S. Selective Metallic Tube Reactivity in the Solution-Phase Osmylation of Single-Walled Carbon Nanotubes. *J. Am. Chem. Soc.* **2004**, *126*, 2073–2081.
39. Nunzi, F.; Mercuri, F.; Sgamellotti, A. The Coordination Chemistry of Carbon Nanotubes: A Density Functional Study through a Cluster Model Approach. *J. Phys. Chem. B* **2002**, *106*, 10622–10633.
40. Nunzi, F.; Mercuri, F.; Angelis, F. D.; Sgamellotti, A.; Re, N.; Giannozzi, P. Coordination and Haptotropic Rearrangement of Cr(CO)<sub>3</sub> on (n,0) Nanotube Sidewalls: A Dynamical Density Functional Study. *J. Phys. Chem. B* **2004**, *108*, 5243–5249.
41. Mercuri, F.; Sgamellotti, A. Functionalization of Carbon Nanotubes with Vaska's Complex: A Theoretical Approach. *J. Phys. Chem. B* **2006**, *110*, 15291–15294.
42. Durgun, E.; Dag, S.; Bagci, V. M. K.; Gülsere, O.; Yildirim, T.; Ciraci, S. Systematic Study of Adsorption of Single Atoms on a Carbon Nanotube. *Phys. Rev. B* **2003**, *67*, 201401.
43. Tairova, G. G.; Krasochka, O. N.; Ponomaryov, V. I.; Kvashina, E. F.; Shvetsov, Y. A.; Lisetsky, E. M.; Kiryukhin, D. P.; Atovmyan, L. O.; Borod'ko, Y. G. Structure, Spectra and Chemical Properties of Ditoluenetitanium. *Transition Met. Chem.* **1982**, *7*, 189–190.
44. Calderazzo, F.; Ferri, I.; Pampaloni, G.; Englert, U.; Green, M. L. H. Synthesis of [Ti( $\eta^6$ -1,3,5-C<sub>6</sub>H<sub>3</sub>Pr<sub>3</sub>)<sub>2</sub>][BAR<sub>4</sub>] (Ar = C<sub>6</sub>H<sub>5</sub>, *p*-C<sub>6</sub>H<sub>4</sub>F, 3,5-C<sub>6</sub>H<sub>3</sub>(CF<sub>3</sub>)<sub>2</sub>), the First Titanium(II) Derivatives. *Organometallics* **1997**, *16*, 3100–3101.

45. Elschenbroich, C.; Bretschneider-Hurley, A.; Hurley, J.; Massa, W.; Wocadlo, S.; Pebler, J.  $\mu$ -[1,1,2,2-Tetrakis( $\eta^5$ -phenyl)-1,2-diphenyldisilane]-divanadium: Long Distance Exchange Interaction Mediated through a  $>$ SiPh-SiPh $<$  Unit. *Inorg. Chem.* **1993**, *32*, 5421–5424.
46. Marchettia, F.; Pampalonia, G. Some New Results on the Fischer–Hafner Synthesis of Vanadium Arenes. *J. Organomet. Chem.* **2006**, *691*, 3458–3463.
47. Choukroun, R.; Lorber, C.; Vendier, L. Reaction of  $V(C_6H_6)_2$  with the Borane Adducts of Malononitrile  $[(C_6F_5)_3B \cdot NCCH_2CN \cdot B(C_6F_5)_3]$  and Water  $[H_2O \cdot B(C_6F_5)_3]$ . *Organometallics* **2007**, *26*, 3604–3606.
48. Eyring, M. W.; Zuerner, E. C.; Radonovich, L. J. Substituent Effects in Bis(arene) Complexes. Structures of Bis(1,4-bis(trifluoromethyl)benzene)chromium(0) Bis(1,3-bis(trifluoromethyl)benzene)chromium(0), and Bis(1-chloro-3-(trifluoromethyl)benzene)chromium(0). *Inorg. Chem.* **1981**, *20*, 3405–3410.
49. Lyssenko, K. A.; Korlyukov, A. A.; Golovanov, D. G.; Ketkov, S. Y.; Antipin, M. Y. Estimation of the Barrier to Rotation of Benzene in the  $(\eta^6-C_6H_6)_2Cr$  Crystal via Topological Analysis of the Electron Density Distribution Function. *J. Phys. Chem. A* **2006**, *110*, 6545–6551.
50. Braga, D.; Maini, L.; Grepioni, F.; Elschenbroich, C.; Paganelli, F.; Schiemann, O. Novel Organometallic Building Blocks for Crystal Engineering. Synthesis and Structural Characterization of the Dicarboxylic Acid  $[Cr^0(\eta^6-C_6H_5COOH)_2]$ , of Two Polymorphs of Its Oxidation Derivative  $[Cr^I(\eta^6-C_6H_5COOH)_2]^+[PF_6]^-$ , and of the Zwitterionic Form  $[Cr^I(\eta^6-C_6H_5COOH)(\eta^6-C_6H_5COO)]$ . *Organometallics* **2001**, *20*, 1875–1881.
51. Braga, D.; Eckert, M.; Fraccastoro, M.; Maini, L.; Grepioni, F.; Caneschi, A.; Sessoli, R. The Hydrogen Oxalate Anion Allows One-Dimensional Columnar Aggregation of Organometallic Sandwich Cations. *New J. Chem.* **2002**, *26*, 1280–1286.
52. O'Hare, D.; Murphy, V.; Bland, A.; Scott, P. X-ray Structure of  $[Mn(\eta-C_6H_5(Me))_2]^+$ . *J. Organomet. Chem.* **1993**, *443*, C37–C38.
53. Ward, M. D.; Johnson, D. C. Electrocrystallization and Structural and Physical Properties of Charge-Transfer Complexes Derived from  $[(\eta^6-C_6Me_6)_2M]^{2+}$  ( $M = Fe, Ru$ ) and TCNQ (TCNQ = tetracyanoquinodimethane). *Inorg. Chem.* **1987**, *26*, 4213–4227.
54. Thompson, M. R.; Day, C. S.; Day, V. W.; Mink, R. I.; Muetterties, E. L. Transition Metal Arene Chemistry. 4. Structural Studies of Cobalt Group Complexes. *J. Am. Chem. Soc.* **1980**, *102*, 2979–2986.
55. Priego, J. L.; Doerrer, L. H.; Rees, L. H.; Green, M. L. H. Weakly-Coordinating Anions Stabilize the Unprecedented Monovalent and Divalent  $\eta$ -Benzene Nickel Cations  $[(\eta-C_5H_5)Ni(\eta-C_6H_6)Ni(\eta-C_5H_5)]^{2+}$  and  $[Ni(\eta-C_6H_6)_2]^{2+}$ . *Chem. Commun.* **2000**, 779–780.
56. Mascal, M.; Kerdelhue, J.-L.; Blake, A. J.; Cooke, P. A. S-Cylindrophanes: From Metal Tweezers to Metal Sandwiches. *Angew. Chem., Int. Ed.* **1999**, *38*, 1968–1971.
57. Shim, D.; Jung, S.-H.; Han, S. Y.; Shin, K.; Lee, K.-H.; Han, J. H. Improvement of SWCNT Transparent Conductive Films via Transition Metal Doping. *Chem. Commun.* **2011**, *47*, 5202–5204.
58. Georgakilas, V.; Gournis, D.; Tzitzios, V.; Pasquato, L.; Guldi, D. M.; Prato, M. Decorating Carbon Nanotubes with Metal or Semiconductor Nanoparticles. *J. Mater. Chem.* **2007**, *17*, 2679–2694.
59. Wildgoose, G. W.; Bankds, C. E.; Compton, R. G. Metal Nanoparticles and Related Materials Supported on Carbon Nanotubes: Methods and Applications. *Small* **2006**, *2*, 182–193.
60. Fujimoto, Y.; Saito, S. Energetics and Electronic Structures of Pyridine-Type Defects in Nitrogen-Doped Carbon Nanotubes. *Phys. E* **2011**, *43*, 677–680.
61. Min, Y. S.; Bae, E. J.; an dU. J. Kim, I. P. A.; Park, W. Growth and Characterization of Nitrogen-Doped Single-Walled Carbon Nanotubes by Water–Plasma Chemical Vapour Deposition. *Nanotechnology* **2007**, *18*, 285601.
62. Min, Y.-S.; Bae, E. J.; Kim, U. J.; Lee, E. H.; Park, N.; Hwang, C. S.; Park, W. Unusual Transport Characteristics of Nitrogen-Doped Single-Walled Carbon Nanotubes. *Appl. Phys. Lett.* **2008**, *93*, 043113.
63. Feng, H.; Ma, J.; Hu, Z. Nitrogen-Doped Carbon Nanotubes Functionalized by Transition Metal Atoms: A Density Functional Study. *J. Mater. Chem.* **2010**, *20*, 1702–1708.
64. Shang, Y.; Zhao, J.-X.; Wu, H.; Cai, Q.-H.; Wang, X.-G.; Wang, X.-Z. Chemical Functionalization of Pyridine-like and Porphyrin-like Nitrogen-Doped Carbon (CN<sub>x</sub>) Nanotubes with Transition Metal (TM) Atoms: A Theoretical Study. *Theor. Chem. Acc.* **2010**, *127*, 727–733.
65. Kolchinski, A. G. Anhydrooligomers of *o*-Aminobenzaldehydes—The Rich Chemistry of the Busch Macrocycles. *Coord. Chem. Rev.* **1998**, *174*, 207–239.
66. Ramasami, T.; Endicott, J. F. Nonadiabatic Effects in Outer-Sphere Electron-Transfer Reactions of Cobalt(III) Complexes: Experimental Probes of Charge-Transfer Perturbations of the Rates of Several Cross-Reactions. *Inorg. Chem.* **1984**, *23*, 3324–3333.
67. Taylor, L. T.; Busch, D. H. Stereospecific Formation of Chelate Sandwich Compounds Derived from *o*-Aminobenzaldehyde and 2-Amino-5-chlorobenzaldehyde by a Metal-Ion-Induced Rearrangement. *Inorg. Chem.* **1969**, *8*, 1366–1371.
68. Sheldon, R. I.; Jircitano, A. J.; Beno, M. A.; Williams, J. M.; Mertes, K. B. Methyl-Substituted Tribenzo[*b,f,j*][1,5,9]-triazacyclododecine with Copper(II) Ion: A Dynamic Jahn-Teller Effect. *J. Am. Chem. Soc.* **1983**, *105*, 3028–3031.
69. Choi, H. C.; Park, J.; Kim, B. Distribution and Structure of N Atoms in Multiwalled Carbon Nanotubes Using Variable-Energy X-ray Photoelectron Spectroscopy. *J. Phys. Chem. B* **2005**, *109*, 4333–4340.
70. Kudashov, A. G.; Okotrub, A. V.; Bulusheva, L. G.; Asanov, I. P.; Shubin, Y. V.; Yudanov, N. F.; Yudanova, L. I.; Danilovich, V. S.; Abrosimov, O. G. Influence of Ni–Co Catalyst Composition on Nitrogen Content in Carbon Nanotubes. *J. Phys. Chem. B* **2004**, *108*, 9048–9053.
71. Xiao, K.; Lui, Y. Q.; Hu, P. A.; Yu, G.; Hu, W. P.; Zhu, D. B.; Liu, X. Y.; Liu, H. M.; Wu, D. X. Electronic Transport Characteristic of an Individual CN<sub>x</sub>/C Nanotube Schottky Junction. *Appl. Phys. A: Mater. Sci. Process.* **2006**, *83*, 53–56.
72. Perdew, J.; Burke, K.; Ernzerhof, M. Generalized Gradient Approximation Made Simple. *Phys. Rev. Lett.* **1996**, *77*, 3865–3868.
73. Vanderbilt, D. Soft Self-Consistent Pseudopotentials in a Generalized Eigenvalue Formalism. *Phys. Rev. B* **1990**, *41*, 7892–7895.
74. Giannozzi, P.; Baroni, S.; Bonini, N.; Calandra, M.; Car, R.; Cavazzoni, C.; Ceresoli, D.; Chiarotti, G. L.; Cococcioni, M.; Dabo, I.; *et al.* Quantum-Espresso: A Modular and Open-Source Software Project for Quantum Simulations of Materials. *J. Phys.: Condens. Matter* **2009**, *21*, 395502.
75. Marzari, N.; Vanderbilt, D.; Vita, A. D.; Payne, M. C. Thermal Contraction and Disorder of the Al(110) Surface. *Phys. Rev. Lett.* **1999**, *82*, 3296–3299.
76. Landauer, R. Electrical Resistance of Disordered One-Dimensional Lattices. *Phil. Mag.* **1970**, *21*, 863–867.
77. Mostofi, A. A.; Yates, J. R.; Lee, Y.-S.; Souza, I.; Vanderbilt, D.; Marzari, N. Wannier90: A Tool for Obtaining Maximally-Localized Wannier Functions. *Comput. Phys. Commun.* **2008**, *178*, 685.
78. Ferretti, A.; Bonferroni, B.; Calzolari, A.; Nardelli, M. B. Wann code, <http://www.wannier-transport.org>.
79. Calzolari, A.; Marzari, N.; Souza, I.; Nardelli, M. B. *Ab Initio* Transport Properties of Nanostructures from Maximally Localized Wannier Functions. *Phys. Rev. B* **2004**, *69*, 035108.